



**HAL**  
open science

## Theoretical study of highly strained InAs material from first-principles modelling: application to an ideal QD

Laurent Pedesseau, Jacky Even, Alexandre Bondi, Weiming Guo, Soline Richard, Hervé Folliot, Christophe Labbé, Charles Cornet, Olivier Dehaese, Alain Le Corre, et al.

### ► To cite this version:

Laurent Pedesseau, Jacky Even, Alexandre Bondi, Weiming Guo, Soline Richard, et al.. Theoretical study of highly strained InAs material from first-principles modelling: application to an ideal QD. Journal of Physics D: Applied Physics, 2008, 41, pp.165505. 10.1088/0022-3727/41/16/165505 . hal-00491451

**HAL Id: hal-00491451**

**<https://hal.science/hal-00491451>**

Submitted on 15 Jun 2010

**HAL** is a multi-disciplinary open access archive for the deposit and dissemination of scientific research documents, whether they are published or not. The documents may come from teaching and research institutions in France or abroad, or from public or private research centers.

L'archive ouverte pluridisciplinaire **HAL**, est destinée au dépôt et à la diffusion de documents scientifiques de niveau recherche, publiés ou non, émanant des établissements d'enseignement et de recherche français ou étrangers, des laboratoires publics ou privés.

# Theoretical study of highly strained InAs material from first- Principles modeling: Application to an ideal QD.

L. PEDESSEAU<sup>a</sup>), J. EVEN, A. BONDI, W. GUO, S. RICHARD, H. FOLLIOT, C.  
LABBE, C. CORNET, O. DEHAESE, A. LE CORRE, O. DURAND and S.  
LOUALICHE.

FOTON-INSA Laboratory, UMR 6082 au CNRS, INSA de Rennes, 20 Avenue des Buttes de  
Coësmes, CS 14315, 35043 Rennes Cedex, France

## Abstract.

We study the properties of highly strained InAs material calculated from first principles modeling using ABINIT packages. We first simulate the characteristic of bulk InAs crystal and compare them with both experimental and density functional theory (DFT) results. Secondly, we focus our attention on the strain effects on InAs crystal with a gradual strain reaching progressively the lattice matched parameters of InP, GaAs and GaP substrates. The final part is dedicated to the study of a hypothetical spherical InAs/GaP quantum dot. The effect of hydrostatic deformations for both InAs Zinc-Blende phase and InAs RockSalt phase is discussed.

**P.A.C.S.** 61.50.-f, 64.70.kg, 71.15.Mb, 71.55.Eq, 73.21.La

---

<sup>a</sup> Corresponding author: [laurent.pedesseau@insa-rennes.fr](mailto:laurent.pedesseau@insa-rennes.fr)

## I. Introduction

The potential of the InAs/GaP heterostructures for the quest of new infrared emitters is the main idea beyond this study on the subject based on first-principles calculation. In the last decade, the InAs material has already been associated to InP or GaAs substrates for the study of new optoelectronic devices [1-3]. In these cases, the formation of quantum dots (QD) in the active zone is related to the large lattice mismatch between InAs and the substrate (3.1% for InAs/InP, and 6.8% for InAs/GaAs). However, the InAs/GaP (10.1%) heterostructures have rarely been considered. For this InAs/GaP association, the lattice mismatch is very large and the effect on electronic properties has to be studied more carefully.

Electronic structures of the InAs/InP and InAs/GaAs interfaces have been studied extensively either in self-consistent density functional theory (DFT) [4-8], k.p calculations [9-14] or tight binding (TB) model [15-19]. DFT calculations only provide to the *maximum maximorum* a couple of hundred atoms in a supercell. On the other hand, the k.p or TB methods are usually used to reach more than thousand atoms. We here study via DFT basic properties of InAs/GaP interfaces in order to spawn input data to the k.p method. To perform it, the first prerequisite is to focus on InAs bulk material. Then we focused on InAs crystal under hydrostatic strain because a lot of experimental studies can be compared to our calculations. The next stage which is not treated here would be to study InAs crystal under biaxial deformations and then InAs/GaP interfaces. DFT simulations have been carried out with the open source ABINIT computer package [20] using a plane-wave basis.

Therefore in this present work, we first compare the properties of InAs in its bulk state with experimental values. Secondly, we study the behavior of InAs crystal under hydrostatic strain. The hydrostatic deformations will be considered up to the large lattice mismatches of 11.2%

corresponding to the lattice parameter of GaP crystal. In the last part, strain relaxation effects are estimated in the case of a spherical InAs inclusion surrounded by a GaAs or a GaP matrix.

## II. Bulk properties of InAs

InAs and GaP bulk crystals are considered with the local density approximation (LDA) as pseudopotential [21]. Convergence tests have been performed with a cutoff equal to 70.0 Ry and up to 160.0 Ry. Actually, a cut-off equal to 70.0 Ry is a good compromise for our simulation. The calculation takes into account the d electron effect. A 8x8x8 k-point grid [22] is chosen and we use first a zinc-blende (ZB) crystal structure for InAs bulk materials. Basic properties of InAs in the ZB bulk state are calculated by DFT method and reported in Table 1 *e.g.* lattice parameter  $\mathbf{a}_0$ , cohesive energy  $\mathbf{E}_{\text{coh}}$ , formation enthalpy  $\Delta\mathbf{H}_f$ , Poisson ratio  $\nu_{100}$ , Young modulus  $\mathbf{Y}_{100}$ , bulk modulus  $\mathbf{B}_0$  and spin-orbit splitting  $\Delta\mathbf{SO}$ . Minimum errors are less than 2% for the calculation of the lattice parameter, the Poisson ratio and the spin-orbit splitting. We compare this DFT calculation with experimental results in ref [23] and other DFT calculation in ref [24, 25]. As usual with LDA pseudopotential, we found more than 3% errors for calculations of the cohesive energy, the formation enthalpy, the Young modulus and the bulk modulus. Indeed, it leads to cohesive energies of solids which are slightly overestimated. The same quantities were evaluated for InAs bulk material in the rocksalt (RS) phase. The main results are the following: the cell parameter and the cohesive energy are smaller for the RS phase. A phase transition is expected at high pressure. Elastic constants  $\mathbf{c}_{11}$ ,  $\mathbf{c}_{12}$  and  $\mathbf{c}_{44}$  are calculated and shown in Table 2. We compare our study with experimental results in ref [26, 27] and other DFT calculation in ref [28]. These elastic constants  $\mathbf{c}_{11}$  and  $\mathbf{c}_{12}$  are well defined for this ZB crystal bulk structure *i.e.* within an error of about 4% which characterizes this method.

## III. Towards huge deformation – highly strained InAs

### Phase Transition from ZB to RS (hydrostatic deformation)

A phase transition from a zinc-blende (ZB) to a rocksalt (RS) structure of InAs has already been investigated in ref [29, 30]. The equilibrium lattice parameter has been computed by minimizing the crystal total energy calculated for different values of lattice constant. Figure 1 represents the total energy as a function of cell volume. From this figure, one can clearly see that the ZB phase is more stable. The equilibrium volume  $V_{\text{ZB}}^0$  for the ZB structure of InAs crystal at zero pressure is about  $379.8 \text{Bohr}^3$  and the equilibrium volume  $V_{\text{RS}}^0$  of the RS structure of InAs is about  $0.802 V_{\text{ZB}}^0$ . The critical pressure for the ZB $\rightarrow$ RS first order phase transition can be calculated by using the “common tangent technique” for both phases [31]. From this tangent (figure 1), we found the volumes *e.g.*  $V_{\text{RS}}^c$  and  $V_{\text{ZB}}^c$  at critical pressure  $P_c$  equal respectively to  $273.2 \text{ bohr}^3$  and  $332.8 \text{ bohr}^3$ . The  $V(P)$  variation for both ZB and RS phases is plotted in figure 2(a) to determine  $P_c$ . The volume discontinuity ( $V_{\text{ZB}}^c - V_{\text{RS}}^c$ ) takes place at the phase transition pressure  $P_c$  equal to 9.5GPa as shown with a vertical line. Another method can be used to spawn  $P_c$  by calculating the Gibbs free energy at  $T=0\text{K}$  ( $G = H - TS = H$ ) for the ZB and RS phases as a function of pressure as illustrated in figure 2(b) *i.e.*  $H_{\text{ZB}}(P_c) = H_{\text{RS}}(P_c)$ . These two methods yield the same value for  $P_c$ . One can compare this result with a calculation done by Christensen using the linear muffin-tin-orbital (LMTO) [32, 33] ( $P_c=7.8 \text{ GPa}$ ), and another DFT calculation done by L. Louail *et al* ( $P_c=8.73 \text{ GPa}$ ) close to our result, and finally with experimental result done by Y.K. Vohra *et al* [34] which measured a transition pressure equal to 7.0 GPa. We may add that the first order phase transition takes place at a critical hydrostatic pressure, which corresponds for the ZB

phase, to a  $V_{ZB}^c$  value between the one of InP equal to  $V_{ZB,InP}^0 = 341.0 \text{ bohr}^3$  and the one of GaAs equal to  $V_{ZB,GaAs}^0 = 304.5 \text{ bohr}^3$ .

### Elastic constants (hydrostatic deformations)

To illustrate the evolution of elastic constants  $c_{11}$ ,  $c_{12}$  and  $c_{44}$  under hydrostatic deformations, we simulate the compression of InAs crystal up to the lattice matching of the GaP crystal. Results are shown on Fig. 3. The most interesting point is that the  $c_{44}$  elastic constant is almost constant from 0 GPa to nearly 30 GPa [35]. The  $c_{44}$  elastic modulus discontinuity at the phase transition is indeed very small.  $c_{11}-c_{12}$  is also almost constant in the ZB phase below the critical pressure  $P_c$ , but it undergoes a large discontinuity at the phase transition. When focusing on the 3 variations of elastic constants due to the phase transition which is equal to  $\Delta c_{11}^c = c_{11}^{RS,c} - c_{11}^{ZB,c} = 115.8 \text{ GPa}$ ,  $\Delta c_{12}^c = c_{12}^{RS,c} - c_{12}^{ZB,c} = -29.8 \text{ GPa}$  and

$\Delta c_{44}^c = c_{44}^{RS,c} - c_{44}^{ZB,c} = 14.1 \text{ GPa}$  then one can say that the variation is huge in the case  $c_{11}$  and the other variations are not so important due to the RS phase where atoms are much condensed in the unit cell and mixes in all faces of the unit cube.

The traditional mechanical stability conditions in cubic crystals on the elastic constants are known as  $c_{11}-c_{12}>0$ ,  $c_{11}>0$ ,  $c_{44}>0$  and  $c_{11}+2c_{12}>0$ . The InAs ZB material follows these conditions up to  $P=60\text{GPa}$ . The elastic constants in table 2 and in table 3 obey to these stability conditions for both structures. The nonlinear behaviour of elastic constants  $c_{\alpha\beta}$  e.g.  $c_{11}$ ,  $c_{12}$  and  $c_{44}$  for a cubic crystal on hydrostatic deformations can be describe by  $c_{\alpha\beta}(P)$  using the quadratic order polynomials function of the pressure P:

$$c_{\alpha\beta}(P) = c_{\alpha\beta} + c'_{\alpha\beta} \cdot P + \frac{1}{2} \cdot c''_{\alpha\beta} \cdot P^2$$

These 3 coefficients are reported in table 4 for InAs either in ZB or in RS phases and compared the coefficient calculated in ref. [35]. For instance,  $c_{\alpha\beta}(P)$  can be written for the ZB phase according to the definition in the pressure interval as follows:

$$\begin{cases} c_{11}(P) = 80.6 + 2.67P + 0.030P^2 \\ c_{12}(P) = 43.7 + 3.13P + 0.039P^2, \\ c_{44}(P) = 36.9 + 0.51P - 0.049P^2 \end{cases}$$

### **Bulk modulus (hydrostatic deformations)**

Our results were used to fit the calculated evolution of the bulk modulus  $B$  as a function of pressure in the ZB phase, using a quadratic non-linear dependence  $B = B_0 + B'_0P + B''_0P^2$ . Our results are shown in figure 3 and reported in table 5 for comparison with experimental results fitted with a linear experimental law ( $B = B_0 + B'_0P$ ) [36-38] and another DFT non-linear calculation [39]. The first result is that the quadratic dependence on pressure is weak in that pressure range. Our calculations are in good agreement with the experimental bulk modulus at zero pressure  $B_0$ , the error is less than 1%. The discrepancy between our linear pressure coefficient  $B'_0$  and the experimental one is larger. We calculated the linear pressure coefficient  $B'_0$  and the nonlinear pressure coefficient  $B''_0$  for InAs ZB crystal only. Actually, the best agreement with the experimental data and with the other DFT calculation is obtained when both pressure coefficients *e.g.* linear and nonlinear are calculated near the equilibrium pressure. It should be pointed out that this linear term in the bulk modulus is necessary to describe correctly the Murnaghan equation of state [40]. Furthermore, one can define related to figure 3, the variation of bulk modulus associated to the transition phase which is equal to  $\Delta B_c = B_c^{RS} - B_c^{ZB} = 18.7 \text{ GPa}$ .

### **Anisotropy coefficient (hydrostatic deformations)**

The anisotropy coefficient  $A$  is usually defined as  $A = (\mathbf{c}_{11} - \mathbf{c}_{12}) / 2\mathbf{c}_{44}$  for a cubic crystal [41]. Note that an ideal isotropic-like mechanical behavior is found for  $A = 1$ . Actually, the  $A$  value is typically equal to 0.5 for most of semiconductor which have a ZB crystal structure. This is also true for InAs at low pressure (figure 4) below the critical pressure  $P_c$ . For pressures larger than 9.5 GPa (in the RS crystal structure), a large step  $\Delta A_c = A_c^{RS} - A_c^{ZB} = 1.3$  arises due to the phase transition. The anisotropy coefficient is much larger in the InAs RS crystal phase than in the InAs ZB crystal phase, however our values are significantly smaller than the ones ( $A=3$ ) found in ref. [30].

### Gap Energies

We have studied the variation of the electronic gap energy of the InAs crystal as a function of the lattice deformation using the LDA. This variation is reported on figure 5 for the ZB phase.

Here is the strain tensor for the hydrostatic deformation (HD):  $\boldsymbol{\epsilon}_{\text{hyd}} = \begin{pmatrix} \delta & 0 & 0 \\ 0 & \delta & 0 \\ 0 & 0 & \delta \end{pmatrix}$  with  $\delta$  an

infinitesimal increment. We defined it as  $HD = \frac{\Delta V}{V} = \boldsymbol{\epsilon}_{xx} + \boldsymbol{\epsilon}_{yy} + \boldsymbol{\epsilon}_{zz} = 3\delta$ . A “negative gap”

(−0.49eV) energy at  $\Gamma$  point is calculated at zero pressure whereas the experimental value is positive 0.42eV. This underestimation is a well known problem of the LDA [42, 43]. In order to improve the LDA simulation, a GW correction of about 0.82eV was found using the many-body perturbation theory implemented in ABINIT packages [44]. The evolution of the whole electronic dispersion pattern shows that all the dispersions bands are moving up due to the compression effect but the conduction band is moving faster than the other bands giving rise to an enhancement of the gap energy. We have also calculated the theoretical deformation potential  $\mathbf{a}$  for small hydrostatic deformations of the ZB lattice. This deformation potential [45] is found equal to −6.2eV in good agreement with experimental results −6.1eV [46-48].

The variation of the direct gap energy ( $E_{\text{gap}}$ ) is in fact linear up to  $HD=36\%$  of hydrostatic



deformations (HD), which is beyond the critical pressure point  $P_c$  where one can define  $HD_c$  equal to 12.4%. The linear behavior of the gap energy is described with LDA calculation as:  $E_{\text{gap}}=0.062HD-0.49$ . The variation of the gap energy is strongly non-linear for hydrostatic deformations larger than 36%. This is due to the coupling between the conduction band lying at low energy with other conduction bands located at higher energies. On the other hand, our study shows that the indirect gap in the X direction decreases as a function of pressure. The transition to an indirect band gap energy is however again observed for a pressure  $P=29.3$  GPa beyond the critical pressure  $P_c$ . For very large hydrostatic deformations ( $>50\%$ ), the InAs crystal in the ZB phase is in a semi-metallic state due to the band dispersion along the X direction. The main interesting point for the RS phase, is that a metallic state is found whatever the pressure. This is again induced by the electronic dispersion along the X direction. On figure 6, we have indeed compared the dispersion bands of InAs crystal either for ZB structure (a) and for RS structure (b) at pressure  $P_c$ . It shows that the phase transition is associated to a very important change in the electronic properties of the InAs crystal. Furthermore, one can define (figure 7) the variation of gap energies in  $\Gamma$  point and in X point associated to the phase transition which are equal to  $\Delta E_{\text{gap,c}}^{\Gamma} = E_{\text{gap,c}}^{\Gamma,RS} - E_{\text{gap,c}}^{\Gamma,ZB} = 0.61\text{eV}$  and to  $\Delta E_{\text{gap,c}}^X = E_{\text{gap,c}}^{X,RS} - E_{\text{gap,c}}^{X,ZB} = -4.42\text{eV}$  respectively. On this figure, we can clearly observe for the InAs ZB crystal that before having a semi metallic state (at the pressure P equal to 29.3GPa) due to the band dispersion along X direction, the transition of phase from InAs ZB crystal to InAs RS crystal provide an increase of the gap energy in  $\Gamma$  point and a drastic decrease of the gap in X point.

#### IV. Hypothetic spherical QDs : effect of elastic relaxation.

In order to investigate the effects of large deformation and polymorphism on a InAs nanostructure, we have used the simple model proposed in ref. [33] for a spherical QD.

Within this model, the initial hydrostatic stress of an InAs inclusion is partially relaxed by the surrounding matrix. The InAs material occupies a spherical cavity embedded in infinitely extended matrix and the strain is relaxed inside and outside the QD. It is possible to assume that a coherent RS island is formed into a ZB like matrix as observed in the PbTe/CdTe system [50]. The number of InAs atoms inside the cavity is then given by  $N = \frac{8V}{a_{matrix}^3}$  in

order to yield coherent interfaces. We may notice that this model neglects a number of effects: surface energies, anisotropy of the elastic constants (lens, pyramid, elongated wire ...) ... Notice that it is however necessary to include the variation of the elastic constants as a function of the lattice parameter in order to take correctly into account the lattice relaxation effect between the inclusion and the matrix [33]. On figure8, these variations are given for the InAs ZB phase and for the GaP material. The relaxed lattice constant  $\mathbf{a}$  of the InAs QD under hydrostatic compression is  $\mathbf{a}_0(\text{QD} - \text{InAs}) = \mathbf{a}_{0,\text{InAs}}(\mathbf{1} - \boldsymbol{\alpha})$ . The deformation  $\boldsymbol{\alpha}$  is determined from the static solution of ref.[33]. The same boundary conditions as F. Grosse and R.

Zimmermann are applied and finally led to  $\boldsymbol{\alpha} = \boldsymbol{\alpha}_0 \frac{c_{44,\text{GaP}}}{c_{44,\text{InAs}} - c_{44,\text{GaP}} + \frac{4}{3}c_{11,\text{InAs}}}$ . The lattice

mismatch is  $\boldsymbol{\alpha}_0 = \frac{(\mathbf{a}_{0,\text{InAs}} - \mathbf{a}_{0,\text{GaP}})}{\mathbf{a}_{0,\text{InAs}}} = 10.1\%$  for the InAs/GaP system using the experimental

values. The relaxed lattice constant  $\mathbf{a}$  of the InAs QD under hydrostatic compression is therefore  $\mathbf{a}_0(\text{QD-InAs})=5.55 \text{ \AA}$ .

Figure 9 presents the calculated energies for a spherical inclusion with a radius equal to 5nm. The internal (cohesive) energy of the ZB spherical inclusion is smaller than the one of the RS one (figure 9(a)). As the lattice mismatch is larger for the ZB inclusion, the elastic energy contribution is larger than for the RS inclusion. By adding the elastic energy without relaxation to a GaP or a GaAs matrix, we found that the RS inclusion is more stable than the

ZB one (figure 9(b)). This is particularly true when the GaP material is used as a barrier material. The results obtained by relaxing the strain, are indicated on the third column (figure 9(c)). The stability order is now reversed by comparison to the unrelaxed case. We may however notice that the energy difference between the RS inclusion and the ZB inclusion is not very large respectively about 150eV for GaAs substrate and about 75eV for GaP substrate. Therefore, the possibility of a RS inclusion or at least phase polymorphism can not be ruled out on the basis of the crude model proposed in this part and this is particularly true for GaP substrate.

## V. Discussion and conclusion

A phase transition is predicted for a hydrostatic deformation as studied and shown in ref [49, 50]. The electronic properties are strongly dependent on the strain state for a highly strained material. Further studies concerning the electronic properties of such a QD could then be interesting in order to answer a number of questions concerning the influences of the bulk material phase transition, the non-linear behavior of the elastic and electronic properties or the interface.

By applying hydrostatic deformations, we have shown that one can predict a phase transition from the InAs ZB crystal to InAs RS crystal at a critical pressure  $P_c$  equal to 9.52GPa. Due to the phase transition, we observed either slight or large discontinuities on elastic constants, on the bulk modulus, and on the anisotropic constant. We presented the dependence of  $\Gamma$  point and X point electronic gap energies for ZB crystal only and that beyond its critical pressure. So, we have a great correspondence with the classical theory. Furthermore, we have focused on band dispersions for both phases at the critical pressure  $P_c$ . For the ZB crystal, we applied a  $HD_c$  of about 12.4% corresponding to  $P_c$  where the gap energy is still direct and not yet semi-metallic along X point direction. Even if the stability of RS crystal above  $P_c$  pressure

spawns a large increase of the gap energy in  $\Gamma$  point one can observe a semi-metallic state for whatever the hydrostatic deformation above  $HD_c$ . For high lattice mismatch, we have also shown in a hypothetical spherical QD that the possibility to obtain a polymorphism is non negligible even if strained relaxation was taken into account. Further study will be focused on interface effect (atomic relaxation).

### **Acknowledgments**

The authors thank Evgeni Penev, and Martin Fuchs for discussions and comments on InAs crystal. We also want to thank Resul Eryigit for his advices about the use of Abinit code. We want to acknowledge the European network of excellence SANDIE for its financial support to this research.

### **References**

- [1] A. Antreasyan, C. Y. Chen, S. G. Napholtz, and D. P. Wilt, *J. Appl. Phys.* **58**, 1686 (1985).
- [2] Y. Matsui and Y. Kusumi, *J. Appl. Phys.* **79**, 6982 (1996).
- [3] C. Cornet, C. Platz, P. Caroff, J. Even, C. Labbé, H. Folliot, A. Le Corre, and S. Loualiche, *Phys. Rev. B* **72**, 035342 (2005).
- [4] T. Ohno, *Phys. Rev. B* **38**, 13191 (1988).
- [5] A. Continenza, S. Massidda, and A. J. Freeman, *Phys. Rev. B* **41**, 12013 (1990).
- [6] S.-H. Ke, R.-Z. Wang, and M.-C. Huang, *J. Appl. Phys.* **77**, 2556 (1995).
- [7] N. Moll, M. Scheffler, and E. Pehlke, *Phys. Rev. B* **58**, 4566 (1998).
- [8] G. Bester, A. Zunger, X. Wu, and D. Vanderbilt, *Phys. Rev. B* **74**, 081305 (2006).
- [9] M. Grundmann, O. Stier, and D. Bimberg, *Phys. Rev. B* **52**, 11969 (1995).

- [10] C. Pryor, Phys. Rev. B **57**, 7190 (1998).
- [11] C. Pryor, Phys. Rev. B **60**, 2869 (1999).
- [12] V. Mlinar, M. Tadić, B. Partoens, and F. M. Peeters, Phys. Rev. B **71**, 205305 (2005).
- [13] C. Cornet, A. Schliwa, J. Even, F. Doré, C. Celebi, A. Létoublon, E. Macé, C. Paranthoën, A. Simon, P. M. Koenraad, N. Bertru, D. Bimberg, and S. Loualiche, Phys. Rev. B **74**, 035312 (2006).
- [14] J. Even, F. Doré, C. Cornet, L. Pedesseau, A. Schliwa, and D. Bimberg, Appl. Phys. Lett. **91**, 122112 (2007).
- [15] N. Shtinkov, P. Desjardins, and R. A. Masut, Phys. Rev. B **66**, 195303 (2002).
- [16] R. Santoprete, Belita Koiller, R. B. Capaz, P. Kratzer, Q. K. Liu, and M. Scheffler, Phys. Rev. B **68**, 235311 (2003).
- [17] J.-Q. Lu, H. T. Johnson, V. D. Dasika, and R. S. Goldman, Appl. Phys. Lett. **88**, 053109 (2006).
- [18] W. Jaskólski, M. Zieliński, Garnett W. Bryant, and J. Aizpurua, Phys. Rev. B **74**, 195339 (2006).
- [19] R. Santoprete, P. Kratzer, M. Scheffler, Rodrigo B. Capaz, and Belita Koiller, J. Appl. Phys. **102**, 023711 (2007).
- [20] X. Gonze, J.-M. Beuken, R. Caracas, F. Detraux, M. Fuchs, G.-M. Rignanese, L. Sindic, M. Verstraete, G. Zerah, F. Jollet, M. Torrent, A. Roy, M. Mikami, Ph. Ghosez, J.-Y. Raty, and D. C. Allan, Comput. Mater. Sci. **25**, 478 (2002).
- [21] N. Troullier, J. L. Martins, Phys. Rev. B **43**, 1993 (1991).
- [22] H. J. Monkhorst and J. D. Pack, Phys. Rev. B **13**, 5188, (1976).
- [23] Y.-A. Burenkov, S.-Y. Davydov, and S.-P. Nikanorov, Sov. Phys. Solid State **17**, 7 (1975).
- [24] S. Q. Wang, and H. Q. Ye, Phys. Stat. Sol. (b) **240**, 45-54 (2003).

- [25] E. Penev, On the theory of surface diffusion in InAs/GaAs(001) heteroepitaxy. PhD thesis, [http://edocs.tu-berlin.de/diss/2002/penev\\_evgeni.pdf](http://edocs.tu-berlin.de/diss/2002/penev_evgeni.pdf), TU Berlin, 2002.
- [26] D. F. Nelson and E. H. Turner. *J. Appl. Phys.* **39**, 3337(1968).
- [27] G. Arlt and P. Quadflieg, *Phys. Stat. Sol.(b)* **25**, 323 (1968).
- [28] G. Bester, X. Wu, D. Vanderbilt and A. Zunger, *Phys. Rev. Lett.* **96**, 187602 (2006).
- [29] A. Mujica and R.J. Needs, *Phys. Rev.* **55**, 9659 (1997).
- [30] L. Louail, D. Maouche and A. Hachemi, *Materials Letters* **60**, 3269 (2006).
- [31] E. Deligoz, K. Colakoglu, Y.O. Ciftci, and H. Ozisik, *Computational Materials Science*, **39**, 533 (2007).
- [32] N.E. Christensen, *Phys. Rev.* **33**, 5096 (1986).
- [33] N.E. Christensen, in: T. Suski, W. Paul (Eds.), *High pressure in Semiconductor Physics I*, Academic Press, 1998 and R.K. Willardson, E.R. Weber (Eds.), *Semiconductors and Semimetals*, Vol. 54.
- [34] Y.K. Vohra, S.T. Weir, and A.L. Ruoff, *Phys. Rev.* **31**, 7344 (1985).
- [35] F. Grosse and R. Zimmermann, *Phys. Rev. B* **75**, 235320, (2007).
- [36] Ozolinsk J., Averkieva G., Ilvinsk A., and Goryuna N.. *Sov. Phys.-Cryst.* **7**, 691 (1963).
- [37] Gerlich D. *J. Appl. Phys.* **34**, 2915 (1963).
- [38] Vuxceovich M. R. *Phys. Stat. Sol.(b)* **54**, 219 (1972).
- [39] P. E. Van Camp, V. E. Van Doren, and J. T. Devreese, *Phys. Rev.* **B41**, 1598, (1990).
- [40] F. D. Murnaghan, *Proc. Nat. Acad. Sci. USA* **30**, 244 (1944).
- [41] C. Zener, *Phys. Rev.* **71**, 12 (1947) 846-851.
- [42] X. Zhu and S.G. Louie, *Phys. Rev.* **B43**, 14142 (1991).
- [43] Z. Zanolli, F. Fuchs, J. Furthmüller, U. von Barth and F. Bechstedt, *Phys. Rev.* **75**, 245121-8 (2007).
- [44] M. Hybertsen and S.G. Louie, *Phys. Rev.* **B30**, 5777 (1984).

- [45] G.E. Pikus and G.L. Bir, *Sov. Phys.-Solid State* **1**, 136 (1959)
- [46] P.-Y. Yu, and M. Cardona, « *Fundamentals of Semiconductors: Physics and Materials Properties.* », Springer, 1996.
- [47] S.-L. Chuang, « *Physics of optoelectronic devices.* Wiley Series in pure and Applied Optics. » Joseph W. Goodman, Series Editor, 1995
- [48] I. Vurgaftman, J. R. Meyer, and L.R. Ram-Mohan. *J. Appl. Phys.* **89**, 5815 (2001).
- [49] R. Leitsmann, L.E. Ramos, and G. Bechstedt, *Phys. Rev.* **74**, 085309-8. (2006)
- [50] W. Heiss, H. Groiss, E. Kaufmann, G. Hesser, M. M. Böberl, G. Springholtz, F. Schaäffler, R. Leitsmann, G. Bechstedt, K. Koike, H. Harada and M. Yano. *J. Appl. Phys.* **101**, 081723 (2007).

## Figure captions

**Figure 1:** Energy variation as a function of the volume for the InAs Zinc-Blende phase (ZB, ●) and the InAs RockSalt phase (RS, ◆). The “common tangent technique” (Tangent, —) provides the two volumes (⊕) which correspond to the phase transition.

**Figure 2:** (a) Pressure versus volume curves for both the InAs ZB phase (●) and the InAs RS phase (◆). The phase transition critical pressure is shown with a vertical line. (b) Gibbs energies versus pressure for both the InAs ZB phase (—) and the InAs RS phase (---).

**Figure 3:** Elastic constants and bulk modulus discontinuities from InAs ZB phase to InAs RS phase ( $C_{11}$ , ◆), ( $C_{12}$ , ■), ( $C_{44}$ , ▲) and ( $B_0$ , ●).

**Figure 4:** Anisotropic constant  $A$  discontinuity from InAs ZB phase to InAs RS phase ( $A_{ZB}$ , ■) and ( $A_{RS}$ , ◆).

**Figure 5:** Dependence of  $\Gamma$  point (◆) and X point (●) electronic gap energies versus hydrostatic deformations of the ZB crystal.

**Figure 6:** Dispersion bands of InAs crystals for ZB structure at the transition pressure  $P_c$  (a), and dispersion bands of InAs crystals for RS structure at the transition pressure  $P_c$  (b).

**Figure 7:** Dependence of  $\Gamma$  point (—) and X point (---) electronic gap energies discontinuities versus hydrostatic pressure from InAs ZB phase to InAs RS phase.



**Figure 8:** Elastic constants of the InAs ZB crystal ( $C_{11}$ ,  $\blacklozenge$ ), ( $C_{12}$ ,  $\blacksquare$ ), ( $C_{44}$ ,  $\blacktriangle$ ) (blue line) and of the GaP crystal ( $C_{11}$ ,  $\blacklozenge$ ), ( $C_{12}$ ,  $\blacksquare$ ), ( $C_{44}$ ,  $\blacktriangle$ ) (red line). The experimental equilibrium lattice constants are given by dashed lines and the lattice constant of the relaxed InAs QD is marked by the full vertical line.

**Figure 9:** Internal cohesive energy  $E_{\text{coh}}$  for a spherical inclusion (radius equal to 5nm) of both InAs ZB (blue) crystal and InAs RS (red) crystal (a) only, then effect on the sum with either the elastic energy  $E_{\text{elas}}$  unrelaxed (b) or relaxed (c) to a GaP (—) or a GaAs (— —) matrix.

FIG. 1.

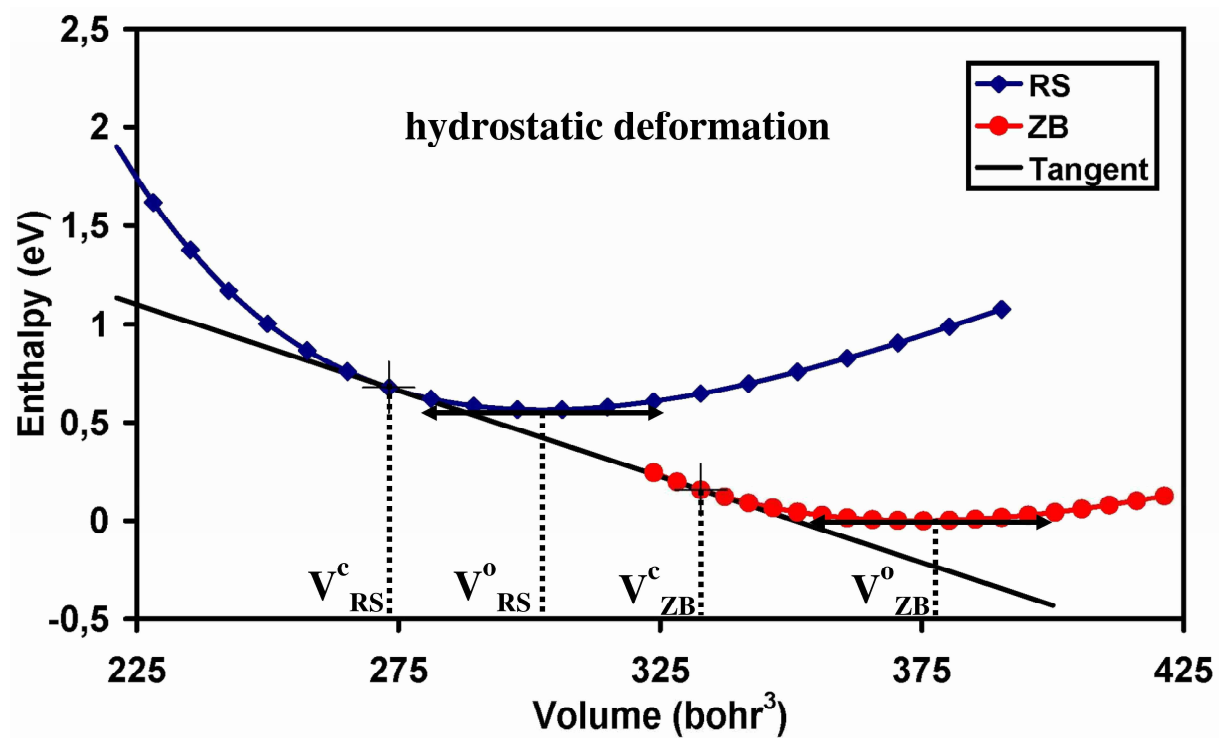


FIG. 2

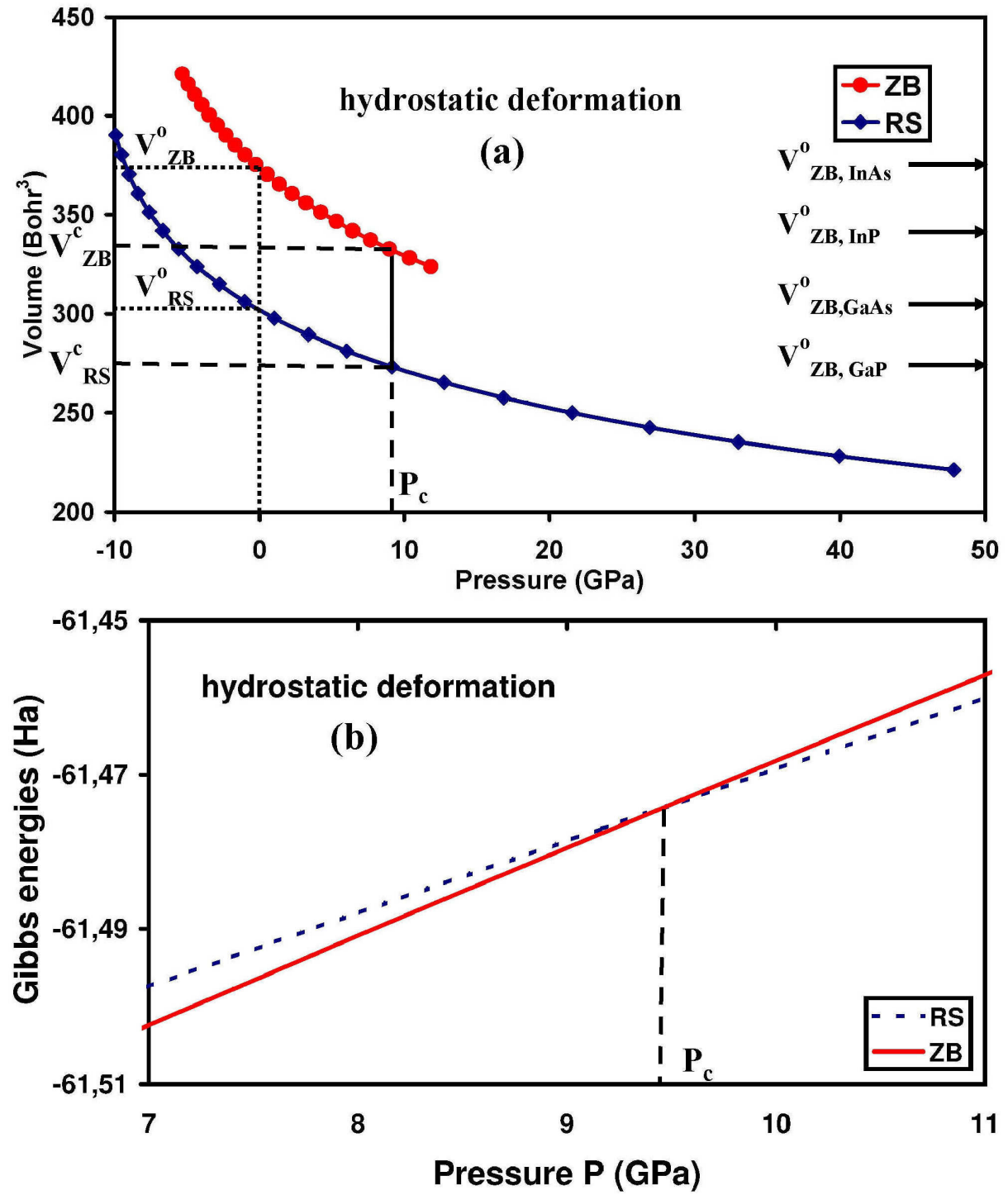


FIG. 3

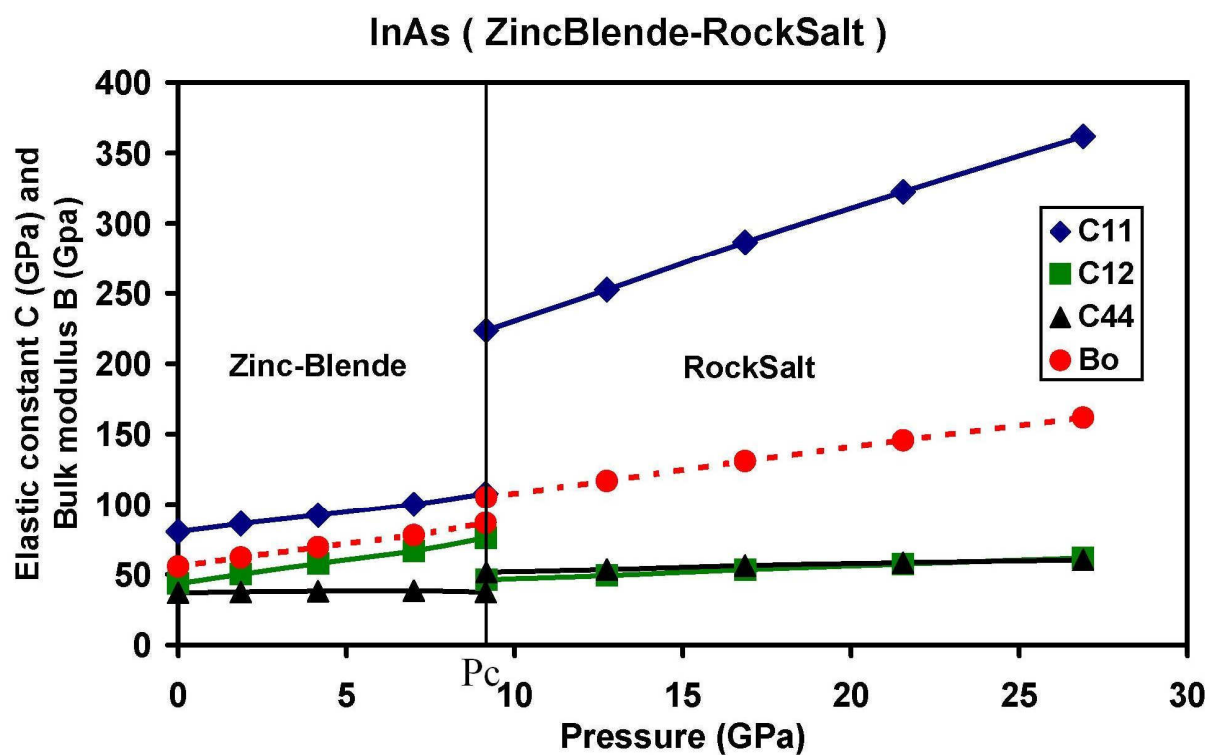


FIG. 4

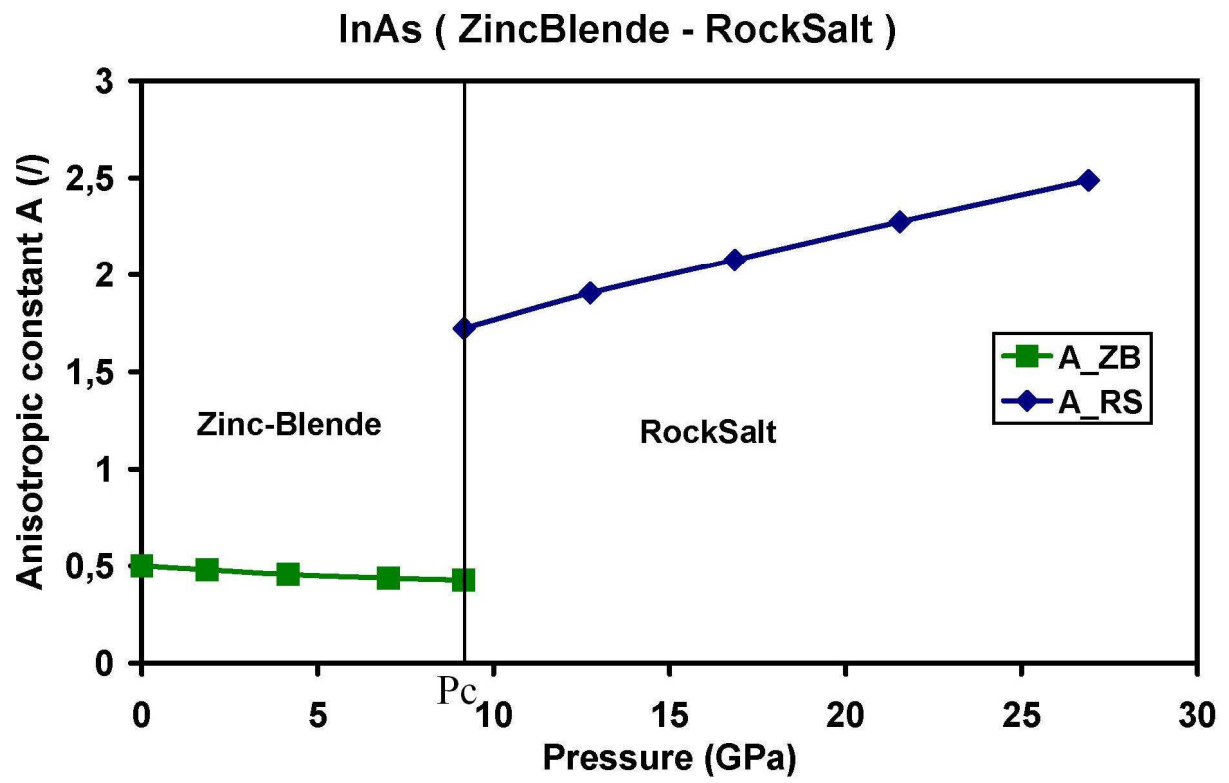


FIG. 5

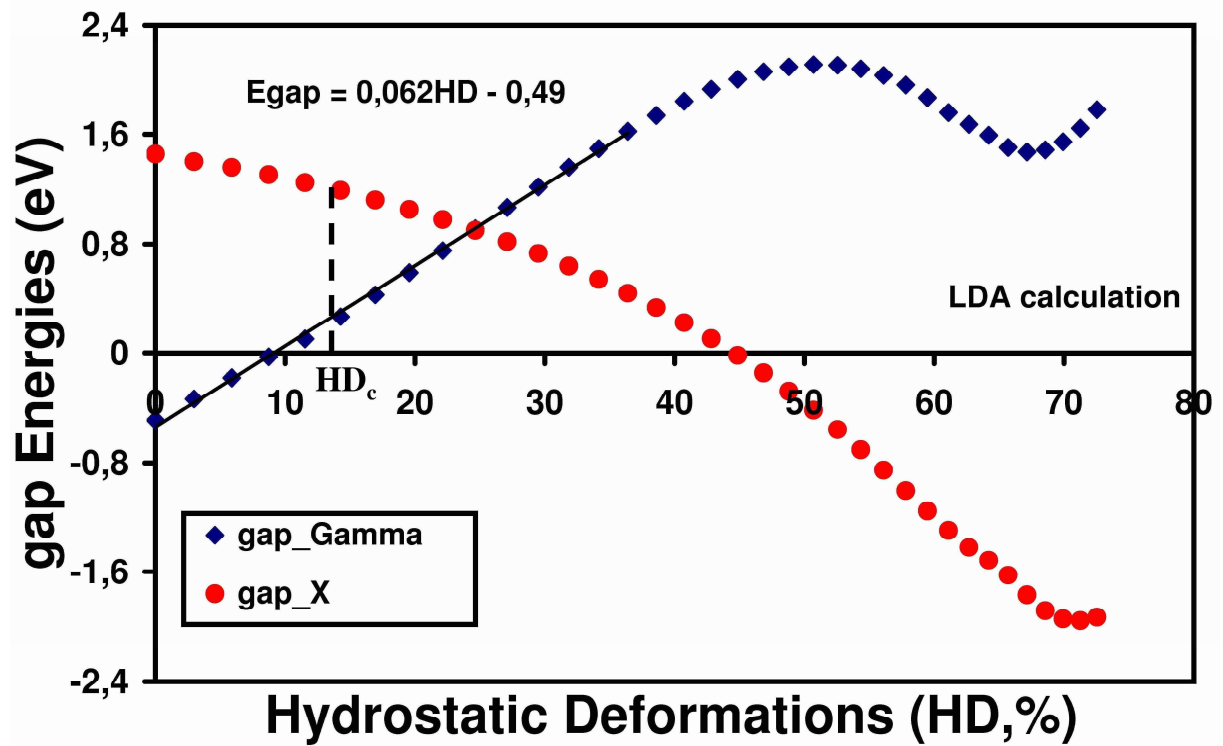


FIG. 6

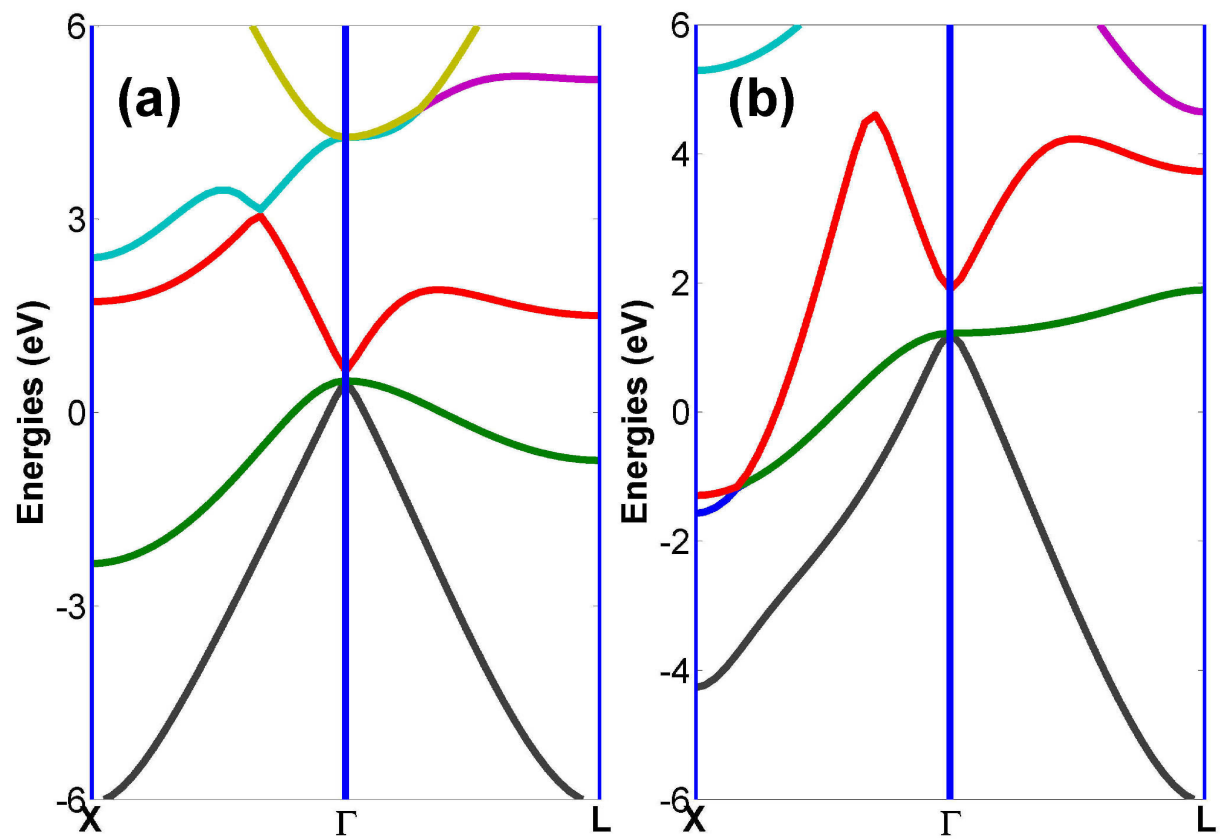


FIG. 7

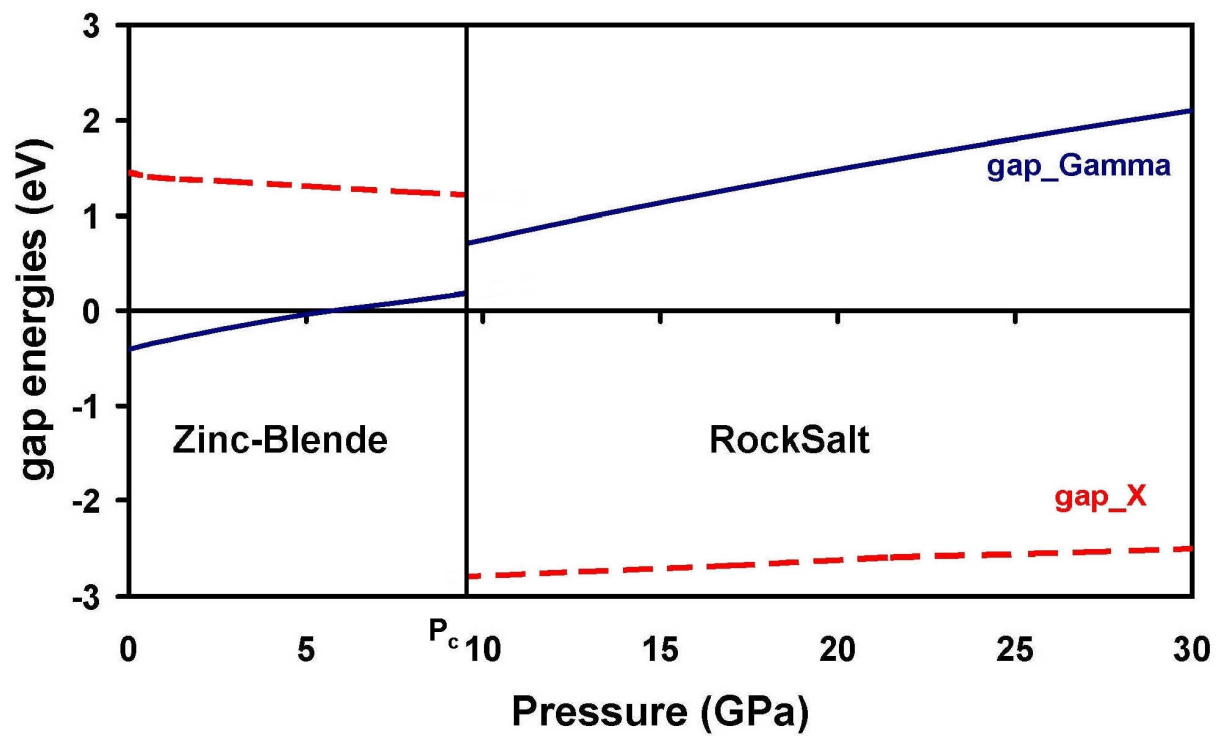




FIG. 8

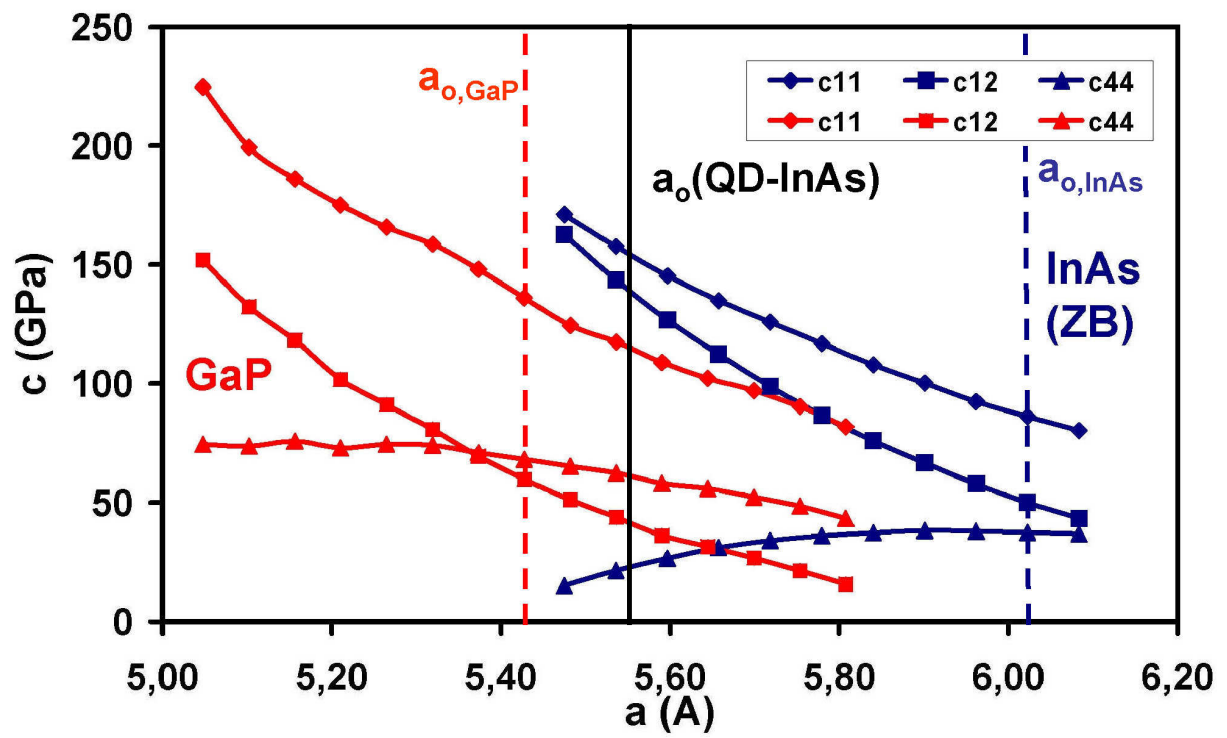
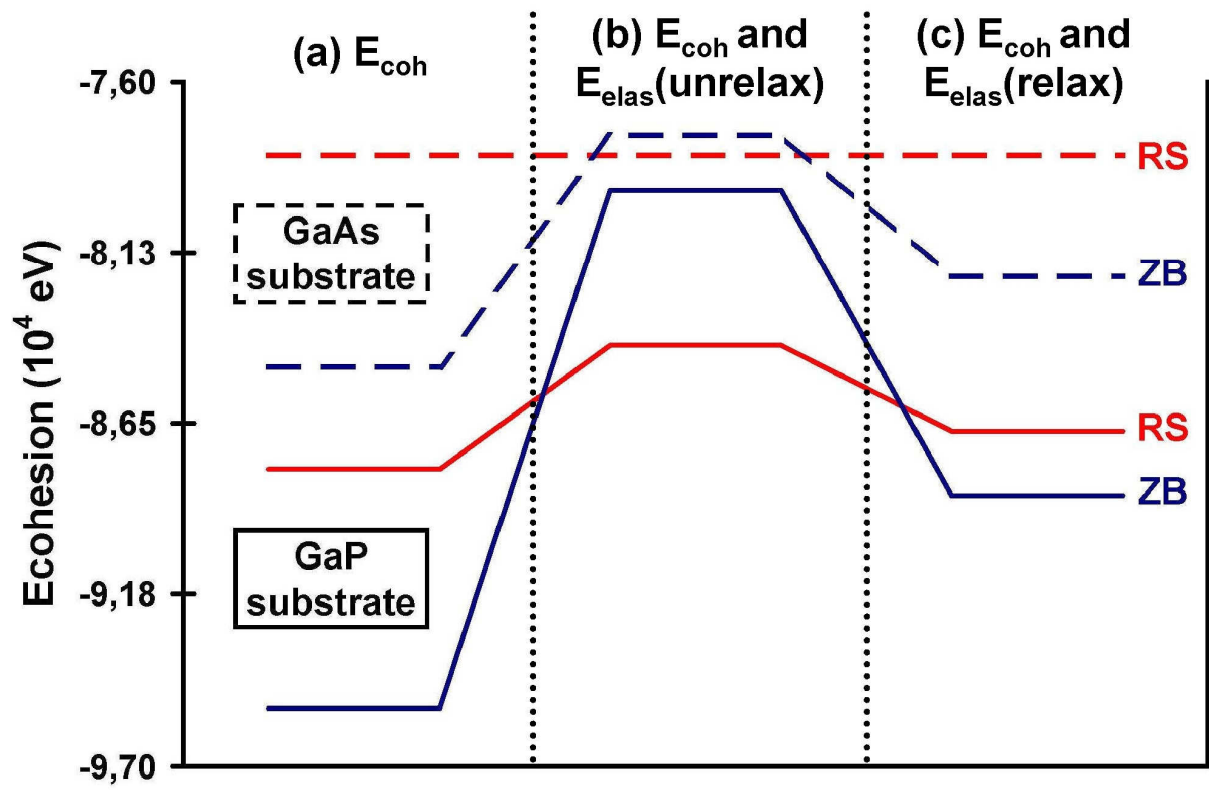


FIG. 9



### Table captions

**Table 1** : Comparison, of the lattice parameter ( $a_0$ , Å), cohesive energies ( $E_{\text{coh}}$ , eV), formation enthalpies ( $\Delta H_f$ , eV), Poisson ratio ( $\nu_{100}$ , /), Young modulus ( $Y_{100}$ , /), Bulk modulus ( $B_0$ , GPa) and the spin-orbit splitting ( $\Delta_{\text{SO}}$ , eV) calculate either for InAs ZB bulk at  $P_0$  pressure or InAs RS bulk at  $P_c$  pressure, with the DFT method and experiment. The values in parenthesis are the percentage error of theoretical data compared to experiment.

**Table 2** : Elastic constants (GPa) for InAs ZB bulk at  $P_0$  pressure, with the DFT method and comparison with experiment. The values in parentheses are the percentage error of theoretical data compared to experiment.

**Table 3** : Elastic constants (GPa) for InAs ZB bulk and RS bulk at  $P_c$  pressure, with the DFT method and comparison with DFT ref L. Louail *et al.*

**Table 4** : The 3 elastic coefficients *e.g.*  $c_{\alpha\beta}$  (GPa),  $c'_{\alpha\beta}$  (/) and  $c''_{\alpha\beta}$  (GPa<sup>-1</sup>) for both InAs ZB bulk and RS bulk with the DFT method and comparison with other DFT ref F. Grosse *et al.*

**Table 5** : Calculated and experimental values of the lattice parameter  $a_0$ (Å), the bulk modulus  $B_0$ (GPa), the linear pressure coefficient  $B'_0$  (/), and the nonlinear pressure coefficient  $B''_0$  (GPa<sup>-1</sup>) of the InAs under hydrostatic deformations.

**TABLE 1**

method		<b>ao</b>	<b>E<sub>coh</sub></b>	<b>ΔH<sub>f</sub></b>	<b>v<sub>100</sub></b>	<b>Y<sub>100</sub></b>	<b>Bo</b>	<b>Δ<sub>SO</sub></b>
<b>InAs</b> <b>(ZB)</b>	present work	6.08 (0.3)	3.64(17)	-0.41(6.8)	0.3516(0.4)	49.42(3.8)	55.51(4.4)	0.386(1.5)
	Other DFT	6.01(0.8)	3.75(21)	-0.38(13.6)	0.35	52.80(2.7)	55.50(4.4)	0.38
	Experiment	6.0585	3.10	-0.44	0.350	51.40	58.07	0.38
<b>InAs</b> <b>(RS)</b>	present work	5.6531	3.36	+0.15	0.17	208	105.3	0.34

**TABLE 2**

method		$c_{11}$ (GPa)	$c_{12}$ (GPa)	$c_{44}$ (GPa)
<b>InAs</b> <b>(ZB, Po)</b>	This study	80.3(3.7)	43.4(4.3)	36.9(6.3)
	<b>other DFT</b>	92.2(10.5)	46.5(2.4)	44.4(12.4)
	<b>Experiment</b>	83.4	45.4	39.5

**TABLE 3**

method		$c_{11}$ (GPa)	$c_{12}$ (GPa)	$c_{44}$ (GPa)	$B_c$ (GPa)	$A_c$ (/)
<b>InAs</b> <b>(ZB, Pc)</b>	This study	107.8	76.0	37.4	86.6	0.42
	<b>other DFT</b>	145	100	50	115	0.45
<b>InAs</b> <b>(RS, Pc)</b>	This study	223.6	46.2	51.5	105.3	1.72
	<b>other DFT</b>	282	63.6	36.4	136.4	3

**TABLE 4**

method			$c_{\alpha\beta}$ (GPa)	$c'_{\alpha\beta}$ (/)	$c''_{\alpha\beta}$ (GPa <sup>-1</sup> )
<b>InAs (ZB)</b>	This study	<b><math>c_{11}</math></b>	80.6	2.67	0.060
	<b>other DFT</b>		78.1	4.05	-0.16
	This study	<b><math>c_{12}</math></b>	43.7	3.13	0.078
	<b>other DFT</b>		48.9	4.60	-0.16
	This study	<b><math>c_{44}</math></b>	36.9	0.51	-0.098
	<b>other DFT</b>		26.2	0.06	-0.038
<b>InAs (RS)</b>	This study	<b><math>c_{11}</math></b>	142.8	9.12	-0.073
	This study	<b><math>c_{12}</math></b>	37.1	1.01	-0.007
	This study	<b><math>c_{44}</math></b>	44.3	0.86	-0.020

**TABLE 5**

<b>InAs</b>	<b><math>a_0(\text{\AA})</math></b>	<b><math>B_0(\text{GPa})</math></b>	<b><math>B'_0 (/)</math></b>	<b><math>B''_0 (\text{GPa}^{-1})</math></b>
<b>our study</b>	6.0834(0.4)	55.51(4.1)	4.1(14.4)	-0.6500
<b>other DFT</b>	5.9019(2.6)	61.90(6.9)	4.4877(6.3)	-0.0750
<b>experiment</b>	6.0583	57.90	4.79	-